P. K. Gantzel, R. A. Sparks, and K. N. Trueblood, UCLA LS4, American Crystallographic Association Program Library (old) No. 317 (revised 1976); Fourier program, C. R. Hubbard, C. O. Quicksall, and R. A. Jacobson, Ames Laboratory Fast Fourier, Iowa State University, 1971; C. K. Johnson, ORTEP, Report No. ORNL-3794, Oak Ridge National Laboratory, Oak Ridge, Tenn., 1965.
(19) S. W. Peterson and H. A. Levy, *Acta Crystallogr.*, **10**, 70 (1957).
(20) P. E. Riley, K. B. Kunz, and K. Seff, *J. Am. Chem. Soc.*, **97**, 537 (1975).
(21) Y. Kim and K. Seff, *J. Am. Chem. Soc.*, **100**, 175 (1978).
(22) D. W. J. Cruickshank, *Acta Crystallogr.*, **2**, 65 (1949).
(23) "International Tables for X-Ray Crystallography", Vol. IV, Kynoch Press, Birmingham, England, 1974, pp 73–87.
(24) Reference 23, pp 149–150.
(25) "International Distances, Supplement", *Chem. Soc., Spec. Publ.*, **No. 18**, M2s (1965).
(26) "Handbook of Chemistry and Physics", Chemical Rubber Publishing Co., Cleveland, Ohio, 1974, p D-157.
(27) Reference 26, p F-201.
(28) Y. Kim and K. Seff, *J. Phys. Chem.*, **82**, 1071 (1978).
(29) Reference 26, p F-198.

# Experimental Evidence for Trapped Valences in the Mixed-Valence Complex μ-Pyrazine-bis(pentaammineruthenium) Tosylate. Electron Paramagnetic Resonance, Magnetic Susceptibility, and Nuclear Magnetic Resonance Results

**Bruce C. Bunker, Russell S. Drago,* David N. Hendrickson,* Robert M. Richman, and Stephen L. Kessell**

*Contribution from the W. A. Noyes Laboratory, University of Illinois, Urbana, Illinois 61801.* *Received October 21, 1977*

**Abstract:** The results of the variable-temperature magnetic susceptibility, EPR, and NMR experiments on salts of $[((NH_3)_5Ru)_2pyr]^{n+}$ ($n$ = 4, 5, 6) and on a salt of $[((NH_3)_5Ru)pyr]^{3+}$ are presented. The unpaired electron in the mixed valence [2,3] oxidation state of the dimer is localized in a ($d_{xz}$, $d_{yz}$) orbital on the Ru(III) center. The electron from the Ru(II) center is transferred through the pyrazine bridge to the other metal site at a rate which is fast on the NMR time scale, but slow on the EPR time scale. The energy barrier to the thermal electron transfer is calculated to be between 3.4 and 6.7 kcal/mol.

Since Creutz and Taube[1] first reported the synthesis of $[((NH_3)_5Ru)_2pyr]^{5+}$, this mixed valence dimer has fostered a great deal of interest and controversy in the literature. Most of the controversy centers on the thermal electron transfer process postulated to occur between the two metal centers in the complex. Accurate rate data for the thermal electron transfer in this simple model system could provide insight into

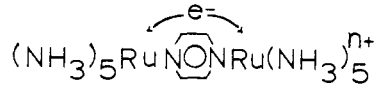


[2,2] [2,3] [3,3]
4+ 5+ 6+

$$[2,3] \underset{}{\overset{k}{\rightleftharpoons}} [3,2]$$

the current theories of electron transfer phenomena. Although many workers have attempted to obtain such rate data for the thermal electron transfer process, the experimental conditions appropriate for observing the phenomenon as a dynamic process have not been found. The unpaired electron either appears to be completely localized or completely delocalized on the time scale of all of the experiments carried out to date, as shown in Table I. The conclusions of several of these experimental studies are based on subtle effects, making it difficult to decide whether the data indicate that the electron is localized or delocalized. Thus, it is not surprising that there is disagreement in the literature concerning the rate of thermal electron transfer.

There is also disagreement about the nature and magnitude of the energy barrier to thermal electron transfer in this interesting complex. Robin and Day[12] have distinguished three classes of mixed-valence complexes based on the extent of overlap between the metal orbitals containing the unpaired electron and the orbitals of the bridging ligand. A similar classification scheme is depicted in Figure 1. If the orbital interactions between the two metal centers through the bridge are negligible (class I), the potential barrier to thermal electron transfer can be defined by two harmonic oscillator potential wells. This vibronic barrier is predicted by the Hush theory[11] to have an energy which is one-fourth the energy of the intervalence transfer band observed in the electronic spectrum of the complex at 1570 nm. If there are extensive metal-metal interactions (class III), the orbital containing the unpaired electron could be delocalized over the entire complex. Here, electronic effects totally remove the vibronic barrier to the electron transfer. The optical and electronic properties of the pyrazine bridged dimer have led Taube and others to classify it as a class II complex described by a localized site molecular orbital scheme in which the vibronic barrier to the electron transfer is lowered to some extent by electronic effects but is not eliminated. Hush argues in favor of a class III designation based on the IR results mentioned in Table I and in light of the fact that the so-called intervalence transfer band shows neither the solvent dependence nor the bandwidth predicted for intervalence transfer transitions by the Hush theory.

Clearly, there is confusion concerning both the molecular orbital description of the mixed valence pyrazine bridged dimer and the rate of thermal electron transfer between the two metal centers. In an attempt to further our understanding of both of these features of this interesting compound, we have carried out a series of EPR, NMR, and magnetic susceptibility ex-

0002-7863/78/1500-3805$01.00/0 

**Table I.** Electron Transfer Rates for [2,3]pyr

| Technique | K Temp. | Sample state | Rate, $s^{-1}$ | $E_{barrier}$ kcal/mol |
|---|---|---|---|---|
| Near IR[1,11] | | Solution | | |
| (Hush) | 300 | Powder | $3 \times 10^{9}$ [a] | 4.5[b] |
| (Hush) | 200 | Powder | $4 \times 10^{7}$ [a] | 4.5[b] |
| (Hush) | 150 | Powder | $7 \times 10^{3}$ [a] | 4.5[b] |
| (Hush) | 80 | Powder | $6 \times 10^{-1}$ [a] | 4.5[b] |
| ESCA[4] | 300 | Powder | $<10^{17}$ | >0.0[a] |
| Raman[6] | 300 | Solution | $<10^{13}$ | >0.0[a] |
| NMR[2] | 302 | Solution | $>10^{6}$ | <9.4[a] |
| Mossbauer[3] | 4 | Powder | $<10^{9}$ | >0.07[a] |
| IR[7] | 300 | KBr pellet | $>10^{13}$ | 0.0[a] |

[a] Calculated using the equation $k = (kT/h)e^{-\Delta E/RT}$. [b] Calculated assuming $E_{barrier} = \frac{1}{4}E_{I.T.}$

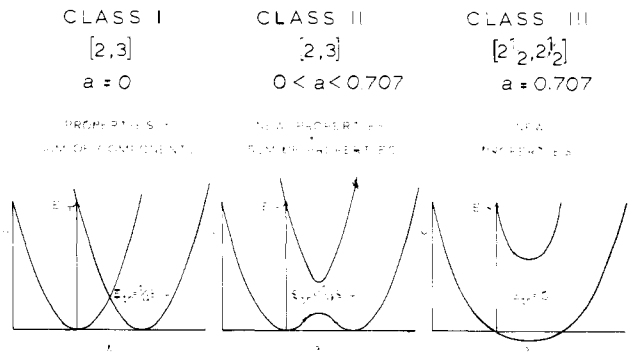


**Figure 1.** Classification scheme for mixed-valence compounds suggested by Robin and Day.[12] Shown at the bottom are the potential energy curves associated with the reaction coordinate for electron transfer for each class. The diagram at the far left under class I shows the vibronic harmonic oscillator potential wells as described in the Hush theory.[11] $E_{IT}$ is the energy of the intervalence transfer band. $E_{th}$ is the magnitude of the energy barrier to thermal electron transfer. $\alpha$ is a measure of the molecular overlap in the ground state of the complex: $\psi_G = (1 - \alpha^2)^{1/2}\Phi_i + \alpha\Phi_j$, where $\psi_G$ is the ground-state wave function and $\Phi_i$ and $\Phi_j$ are the wave functions for the donor-acceptor components of the mixed valence system.

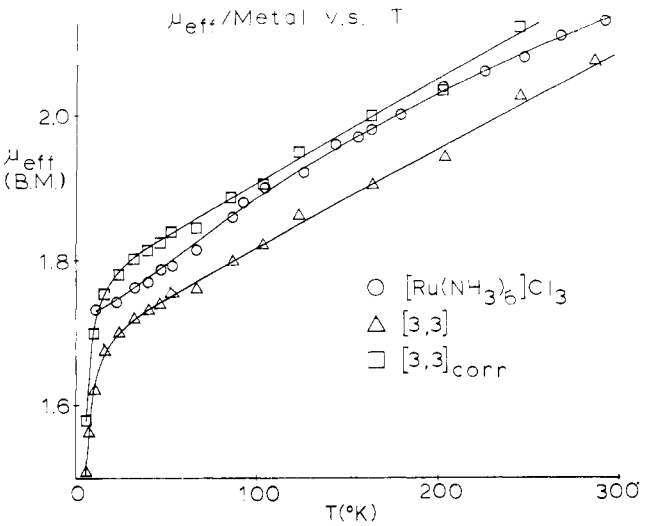


**Figure 2.** Magnetic susceptibility results as a function of temperature for the [3,3]pyr dimer. The curve designated [3,3] shows the actual data obtained for the sample. $[3,3]_{cor}$ shows the data corrected for metal content indicated by elemental analysis. Data for $[Ru(NH_3)_6]Cl_3$ are shown for purposes of comparison.

periments on all three stable oxidation states of the pyrazine bridged dimer and on $[((NH_3)_5Ru)pyr]^{3+}$.

## Results and Discussion

Variable-temperature magnetic susceptibility data have been collected for one $[((NH_3)_5Ru)_2pyr]^{6+}$ salt. These data, in conjunction with variable-temperature EPR results on both the [2,3]- and [3,3]pyrazine bridged dimers and the Ru(III) pyrazine monomer, provide the fundamental information needed to characterize the ground-state molecular orbital of the [2,3]pyr compound. It will be shown that the EPR and NMR results together provide information concerning the rate of thermal electron transfer in the complex.

**Magnetic Susceptibility.** Variable-temperature magnetic susceptibility data were obtained for a sample of $[((NH_3)_5Ru)_2pyr](OTs)_6$, where $OTs^-$ is the tosylate anion ($p$-$CH_3C_6H_4SO_3^-$). These data are given in Table II and are illustrated in Figure 2. The data for this [3,3]pyr compound are in agreement with those reported by Treitel[5] down to liquid nitrogen temperatures. The $\mu_{eff}$ vs. temperature curve in Figure 2 clearly indicates that down to 15 K there is no sign of an antiferromagnetic exchange interaction between the two unpaired electrons, one at each Ru(III) center. The break in the curve at 15 K is indicative either of a very weak antiferromagnetic interaction with $|J| <$ ca. 0.2 $cm^{-1}$ or of slight intermolecular interactions commonly observed in essentially noninteracting monomeric samples. Data would have to be collected to temperatures below 4 K to possibly ascertain the cause of the decrease in $\mu_{eff}$ at low temperatures. In any case, it is apparent that there is a negligible antiferromagnetic exchange interaction in the [3,3]pyr species. The significance of this result as it relates to an understanding of the thermal electron transfer in the [2,3]pyr species is best understood by first looking at its significance in describing the ground state of the [3,3]pyr species.

Two extreme descriptions of the ground state of the [3,3]pyr dimer are shown in Figure 3. For the case where there is considerable overlap between the metal orbitals and the pyrazine bridge (right side of Figure 3), the degenerate orbitals on the two metal centers containing the unpaired electrons interact strongly to give a bonding and nonbonding pair of orbitals. At low temperatures, the two unpaired electrons pair up in the bonding molecular orbital, making the complex diamagnetic. The parameter $J$ obtained from the magnetic susceptibility results is a measure of the energy separation between this diamagnetic singlet ground state and the lowest excited state, which is a triplet. The greater the overlap between the metal orbitals and the bridge is, the greater the singlet-triplet energy separation is, and the larger the $J$ value measured in the susceptibility experiments will be. The small $J$ value obtained for the [3,3]pyr salt indicates that the other limiting description shown in Figure 3 is present. The orbital overlap between the two metal centers, as propagated by the pyrazine bridge, is so small that the two $[(NH_3)_5Ru]^{3+}$ moieties behave as isolated monomeric species with a $\mu_{eff}/Ru = 1.73\ \mu_B$ at low temperatures. The negligible $J$ value obtained for the [3,3]pyr dimer shows that the overlap between the Ru(III) centers and the

**Table II.** Magnetic Susceptibility Data

| | $[Ru(NH_3)_6]Cl_3$[a] | | $[(NH_3)_5Ru\text{-pyr-}Ru(NH_3)_4](OTs)_6$[b] | |
|---|---|---|---|---|
| $T$, K | $10^2\chi_M$, cgsu | $\mu_{eff}$/Ru, $\mu_B$ | $10^2\chi_M$, cgsu | $\mu_{eff}$/Ru, $\mu_B$ |
| 285.5 | 0.182 | 2.04 | 0.378 | 2.08 |
| 244.6 | 0.208 | 2.02 | 0.420 | 2.03 |
| 224.1 | 0.228 | 2.02 | 0.450 | 2.01 |
| 203.7 | 0.247 | 2.01 | 0.488 | 1.99 |
| 162.8 | 0.302 | 1.98 | 0.577 | 1.94 |
| 143.5 | 0.337 | 1.96 | 0.636 | 1.91 |
| 122.5 | 0.384 | 1.94 | 0.709 | 1.86 |
| 102.8 | 0.441 | 1.90 | 0.804 | 1.82 |
| 86.1 | 0.503 | 1.86 | 0.940 | 1.80 |
| 65.7 | 0.627 | 1.82 | 1.18 | 1.76 |
| 52.0 | 0.772 | 1.79 | 1.48 | 1.76 |
| 45.5 | 0.879 | 1.79 | 1.67 | 1.74 |
| 38.6 | 1.02 | 1.77 | 1.94 | 1.73 |
| 31.4 | 1.23 | 1.76 | 2.36 | 1.72 |
| 23.1 | 1.65 | 1.75 | 3.12 | 1.70 |
| 21.4 | 1.77 | 1.74 | 3.36 | 1.70 |
| 17.7 | 2.12 | 1.74 | 4.00 | 1.68 |
| 14.9 | 2.51 | 1.73 | 4.69 | 1.67 |
| 14.0 | 2.68 | 1.73 | 4.95 | 1.66 |
| 13.2 | 2.84 | 1.73 | 5.17 | 1.65 |
| 12.3 | 3.03 | 1.73 | 5.49 | 1.64 |
| 11.4 | 3.26 | 1.73 | 5.87 | 1.64 |
| 10.5 | 3.57 | 1.73 | 6.35 | 1.63 |
| 9.5 | 3.95 | 1.73 | 6.90 | 1.62 |
| 8.8 | 4.26 | 1.73 | 7.34 | 1.61 |
| 7.7 | 4.88 | 1.73 | 8.08 | 1.58 |
| 6.8 | 5.55 | 1.74 | 9.13 | 1.58 |
| 5.8 | 6.55 | 1.74 | 10.5 | 1.56 |
| 5.1 | 7.60 | 1.76 | 11.1 | 1.51 |

[a] Diamagnetic correction used: $-179 \times 10^{-6}$ cgsu. [b] Diamagnetic correction used: $-713 \times 10^{-6}$ cgsu.

pyrazine bridge orbitals is negligible. The complex is better described by a localized site molecular orbital scheme than one which involves delocalization over the entire complex.

The knowledge of the negligible overlap between the Ru(III) orbital containing the unpaired electron and the pyrazine bridge orbitals in the [3,3]pyr complex can be used to describe the ground state and thermal electron transfer of the [2,3]pyr complex by employing a molecular orbital model developed by Ratner[13] for describing the thermal electron transfer process in a mixed-valence species. The mixed-valence species, $(NH_3)_5Ru\text{-pyr-}Ru(NH_3)_5^{5+}$, is considered to be composed of three molecular fragments, the pyrazine bridge B, the $(NH_3)_5Ru^{2+}$ moiety $L_1$ and the $(NH_3)_5Ru^{3+}$ moiety $L_2$. Thermal electron transfer from $L_1$ to $L_2$ via B is treated by a perturbation treatment. The rate of through-bridge transfer is given by the following equation:

$$k_{L_2 \leftarrow L_1} = \frac{2\pi}{\hbar}(H^1_{BL_1}H^1_{BL_2})^2(\hbar\omega_{BL_1})^{-2} \times \left\{\delta(\hbar\omega_{L_1L_2}) + \left(\frac{\omega_{BL_1}}{\omega_{L_1}\omega_{L_2}}\right)^2[\delta(\hbar\omega_{L_1B})]\right\} \quad (1)$$

The major term in this equation is the first term, and for simplicity eq 1 can be rewritten as

$$k \propto \frac{2\pi}{\hbar}(H^1_{BL_1}H^1_{BL_2})^2(\hbar\omega_{BL_1})^{-2} = \frac{2\pi}{\hbar}\Delta^2_{L_1L_2} \quad (2)$$

The parameter $\Delta_{L_1L_2}$ is called the effective bonding overlap integral between the Ru(II) center, $L_1$, and the Ru(III) center, $L_2$. The larger this overlap integral is, the more electronic effects have lowered the vibronic barrier to thermal electron transfer, and the faster the rate of intramolecular electron transfer will be. The effective bonding overlap integral is the

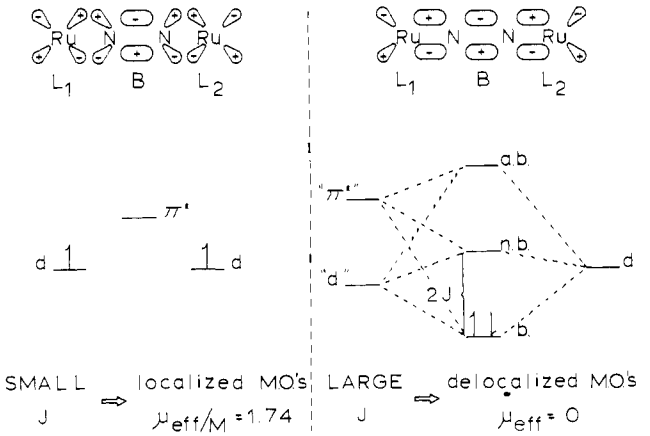


**Figure 3.** Magnetic exchange interactions expected for the [3,3]pyr dimer as a function of the effective molecular orbital overlap between the metal centers and the pyrazine bridge. A small $J$ would be expected if the overlap was negligible and the metal centers were isolated from one another as shown on the left. A large $J$ would be expected if the odd electrons on the two $d^5$ metal centers paired up in a bonding molecular orbital having significant pyrazine $\pi^*$ character as shown on the right.

product of three parameters. The parameter $H^1_{BL_1}$ is the "tunneling integral" between the Ru(II) center and the bridging pyrazine, and $H^1_{BL_2}$ is the "tunneling integral" between the Ru(III) center and the bridge. Both of these integrals depend primarily on the bonding overlap between the bridge and metal orbitals. The term in the denominator, $\hbar\omega_{BL_1}$, is the energy level difference between the unfilled MO regional function of the bridge and the regional acceptor orbitals in the Ru(II) and Ru(III) centers.

The magnetic susceptibility results on the [3,3]pyr dimer indicate that the bonding overlap between the Ru(III) center and the bridge is negligible. This means that $H^1_{BL_2}$ is very small, which should make the entire effective bonding overlap integral, $\Delta_{L_1L_2}$, small as well, even if there is considerable overlap between the Ru(II) center and the bridge. The unpaired electron has no effective electronic pathway for short circuiting the vibronic barrier to electron transfer if it cannot get from the pyrazine bridge to the Ru(III) center via an electronic pathway provided by significant ligand-metal overlap. Therefore, if we can demonstrate that the overlap between the Ru(III) center and the bridging pyrazine is not changed significantly in going from the [3,3]pyr dimer to the [2,3]pyr dimer, we will have established that a localized site class II description is appropriate for describing the ground state of the [2,3]pyr species by our magnetic susceptibility results. The EPR spectra of these two species can tell us whether or not this orbital overlap is changed significantly.

**EPR Results.** Representative EPR spectra obtained for the [2,3]- and [3,3]pyrazine bridged dimers at temperatures between 8 and 50 K are reproduced in Figure 4. The resonance observed for the $Ru^{III}$pyr monomer is identical in appearance with that shown for the [3,3]pyr dimer. The signals for the monomer and the [3,3] dimer are characterized by a single $g$ value of 2.68. No ruthenium hyperfine is observed. In the absence of significant metal hyperfine interactions, the effective spin Hamiltonian for an isolated $S = 1/2$ low-spin $d^5$ Ru(III) metal center in an axial crystal field is

$$H = g_\parallel\beta H_Z S_z + g_\perp\beta(H_X S_X + H_Y S_Y) \quad (3)$$

For this Hamiltonian, two EPR resonances are expected corresponding to $g_\parallel$ and $g_\perp$, with the more intense resonance being associated with $g_\perp$ due to statistical considerations. The observed signal is assigned to the $g_\perp$ component of the spectrum. As we shall see later, the $g_\parallel$ signal is not observed because $g_\parallel$ is less than 0.66, and can only be detected using magnetic fields

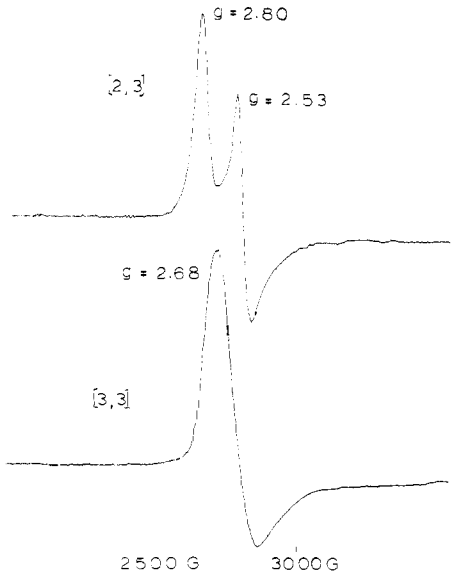


Figure 4. EPR spectra of the [2,3]- and [3,3]pyrazine bridged dimers. Spectra shown are for $Me_2SO$: glycerol frozen solution samples at 24 K.

in excess of the maximum field of 10 000 G attainable on our EPR instrumentation. The EPR signal reported in the literature for $Ru(en)_3^{3+}$ [14] is almost identical with that seen here for the $Ru^{III}$pyr monomer and the [3,3]pyr dimer. The $g_\perp$ resonance for $Ru(en)_3^{3+}$ centered at $g = 2.65$ shows the same asymmetric shape seen here. A $g_\parallel$ value for $Ru(en)^{3+}$ of 0.33 was deduced using single-crystal EPR techniques, since no $g_\parallel$ feature was observable in the EPR spectrum.

The spectrum for mixed-valence $[((NH_3)_5Ru)_2pyr](OTs)_5$ is characterized by two resonances in the $g_\perp$ region. The $g_\perp$ signal is centered at $g = 2.66$ and is apparently split into two resonances at 2.80 and 2.53 corresponding to the $g_x$ and $g_y$ signals. This splitting is probably due to asymmetrical packing of the anions and/or solvent molecules forming the outer coordination sphere around each metal center in the dimeric cations. For several reasons, this interpretation is more reasonable than assigning the two peaks to two distinct ruthenium species having axial symmetry. First of all, although the position of the center of the resonance at $g = 2.66$ is unaffected by the method of sample preparation, the magnitude of the splitting between "$g_x$" and "$g_y$" changes. It is much larger for the $Me_2SO$-glycerol frozen solution samples than for the pure and doped powders, which show $g_x$ and $g_y$ values of 2.72 and 2.60. Secondly, in samples of [2,3] made by recrystallizing [2,2] in the presence of [3,3], no signals are present in either the [2,2] or [3,3] starting materials which can account for the [2,3] signal in terms of impurities. Finally, it seems unlikely that the signal observed for the [2,3] sample is merely a highly resolved [3,3] signal due to dilution of the paramagnetic [3,3] species in a diamagnetic [2,2] lattice. The line widths of the [2,3] and [3,3] resonances are not significantly different at low temperatures (see Figure 4), the intensity of the [2,3] signal parallels the intensity of the intervalence transfer band associated with the [2,3] species, and the conproportionation constant of $10^6$ reported in the literature[16] for the reaction

$$[2,2] + [3,3] \rightleftarrows [2,3]$$

suggests that the concentration of [3,3] in the lattice should be negligible when compared to the concentration of [2,3].

These results for the [2,3]pyr dimer are not in agreement with those reported earlier by Treitel,[5] although his results on the [3,3] system are in fair agreement with ours. For the [2,3] system, he reports a signal observable at room temperature having a $g_\perp = 2.32$ and a $g_\parallel = 2.04$. The intensity of his signal is reported to decay with time, although no change in intensity is observed in the intervalence transfer band associated with the [2,3]pyr dimer. This observation indicates that the species observed in the reported EPR experiments is not [2,3] species.

The $g$ values obtained in our experiments for the three ruthenium compounds described above indicate that the presence of a metal center on the far end of the pyrazine bridge does little or nothing to perturb the orbital environment on the Ru(III) center containing the unpaired electron. No change in $g$ value is detected in going from the $Ru^{III}$pyr monomer to the [3,3]pyr dimer. The difference in average $g_\perp$ value of 0.02 between the [3,3]pyr dimer and the [2,3]pyr dimer is on the same order of magnitude as the experimental error in the $g$ value determination. It has already been demonstrated via the magnetic susceptibility results on the [3,3]pyr dimer that the orbital overlap between the Ru(III) center and the pyrazine bridge is negligible in that species. These EPR results indicate that this overlap is negligible in the [2,3]pyr dimer as well, since the $g$ values observed for the [2,3] and [3,3] species are almost identical. This verifies the conclusion that the [2,3] dimer is a class II localized site complex.

The $g$ value for the [2,3]pyr dimer can also be used to determine what d orbitals are occupied by the unpaired electron on the localized Ru(III) center in the complex. Knowing what these orbitals are and how they are oriented with respect to the $\pi$ and $\pi^*$ orbitals of the pyrazine bridge could tell us a great deal about the nature of the energy barrier to thermal electron transfer between the metal sites and perhaps provide some insight into the mechanism of electron transfer.

General theoretical expressions developed in the literature by Stevens,[17] Kamimura,[18] Bleaney and O'Brien,[19] and others for the $g$ values of a localized low-spin $d^5$ metal can be applied to the $g$ values obtained for the [2,3]pyr dimer. These expressions relate the observed $g$ values to the splitting of the octahedral $^2T_{2g}$ ground state under the combined effects of axial distortions and spin-orbit coupling perturbations. In a previous report from this laboratory these expressions were used to establish the ground state of a series of trisdiimine complexes including tris bipyridyl and tris 1,10-phenanthroline complexes of iron, ruthenium, and osmium.[20,21] These equations appear in their simplest form as

$$g_\parallel = 2|(1 + k)\cos^2\alpha - \sin^2\alpha|$$
$$g_\perp = 2|\sqrt{2k}\cos\alpha\sin\alpha + \sin^2\alpha| \qquad (4)$$

where $\tan 2\alpha = \sqrt{2}\,(1/2 - \Delta/\lambda)^{-1}$. The axial field parameter $\Delta$ is the energy difference between the $^2B_{2g}$ state and the $^2E_g$ state which arise from the octahedral $^2T_{2g}$ ground state due to tetragonal distortions in the octahedral coordination sphere about the metal center. It is defined as positive when the $^2B_{2g}$ state is lowest in energy and negative when the $^2E_g$ state is lowest. The parameter $\lambda$ is the spin-orbit coupling constant for the electronic state, and is negative for a low-spin $d^5$ system due to the hole formalism. The parameters $\Delta$ and $\lambda$ are a measure of the splitting of the octahedral $^2T_{2g}$ ground state into three Kramer's doublets, having energies

$$W_0 = -\Delta/3 - \lambda/2$$
$$W_\pm = 1/2[\Delta/3 + \lambda/2 \pm (\Delta^2 + \Delta\lambda + {}^9/_4\lambda^2)^{1/2}] \qquad (5)$$

These Kramers doublets are shown in Figure 5. The observed EPR transition is between the magnetically split levels of the ground state doublet. The parameter $k$ is the orbital reduction factor

$$k = \frac{\langle\phi|L|\phi\rangle}{\langle d|L|d\rangle} \qquad (6)$$

and is used to correct for deviations in the crystal field model

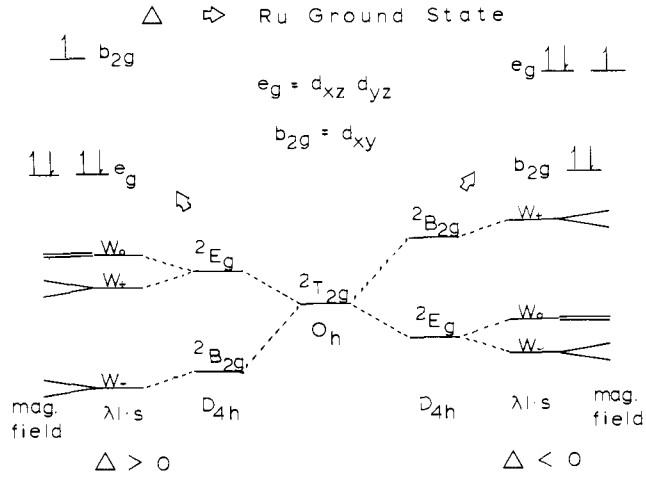


**Figure 5.** Energy level diagram and d orbital splitting patterns expected for a low-spin $d^5$ center as a function of the sign of the tetragonal field parameter Δ. The parameters Δ and λ measure the splitting of the octahedral $^2T_{2g}$ ground state into three Kramer's doublets having energies $W_0 = -\Delta/3 - \lambda/2$, $W_\pm = \frac{1}{2}[\Delta/3 + \lambda/2 \pm (\Delta^2 + \Delta\lambda + \frac{9}{4}\lambda^2)^{1/2}]$. The parameter λ is negative for a $d^5$ system due to the hole formalism. Note that for both positive and negative values of Δ, the degeneracy of the ground-state doublet is removed under the influence of an applied magnetic field, giving rise to the observed EPR transition.

introduced by covalency and other effects. Normal values for $k$ are $\leq 1$, but exceptions are not uncommon.[20,21]

Plots of $g_\parallel$ and $g_\perp$ as a function of Δ and λ are shown in Figure 6 for orbital reduction factors of 1.0 and 1.1. These curves show that for a $g_\perp$ value of 2.68, a $g_\parallel$ value of less than 0.66 is to be expected, in agreement with the experimental observations. They also indicate that the sign of the axial field parameter is negative, and of the same order of magnitude as the spin-orbit coupling constant. Assigning a value of $-1050$ $cm^{-1}$ to λ for Ru(III)[25] and a value of $-945$ $cm^{-1}$ to Δ (assuming $\Delta/\lambda = 0.9$) allows us to calculate approximate energies for the three Kramer's doublets:

$$W_0 = 210\ cm^{-1},\ W_+ = 940\ cm^{-1},\ W_- = -1150\ cm^{-1}$$

As shown in Figure 5, a negative axial field parameter is indicative of the ground state $^2E_{2g}$ which is the result of having the unpaired electron in the $e_g$ orbital set consisting of $d_{xz}$ and $d_{yz}$. Subsequent to our assignment of this ground state, a report of the crystal structure of the [2,3]pyr dimer appeared[8] which shows that there is an axial compression of the molecule along the $z$ axis containing the pyrazine ligand. Such a distortion is consistent with our ground-state assignment. The crystal structure also indicates that the plane of the pyrazine molecule bisects the planes containing the cis ammonias on the ruthenium metal centers. As shown in Figure 7, this means that the unoccupied π* molecular orbitals on the bridge are oriented so that the π density on the pyrazine nitrogens lies between the lobes of the $d_{xz}$, $d_{yz}$ orbital sets on the metals. The symmetry of these orbitals allows for overlap between the $d_{xz}$, $d_{yz}$ orbitals and the pyrazine π and π* orbitals, but the extent of overlap predicted for this orientation should be less than for the orientation used by Day[10] in his calculations of the valence delocalization coefficients for the [2,3]pyr dimer. His calculations are based on the assumptions that the $d_{yz}$ orbital is in the same plane as the π lobes on the pyrazine nitrogens and that the tetragonal distortions from octahedral symmetry occur along the $y$ rather than the $z$ axis. His conclusion is that the hole in Ru(III) is delocalized onto the Ru(II) in the ground state by approximately 1%. Our EPR results, in conjunction with the crystal structure results, indicate that the orbital mixing predicted using an analysis such as Day's is an overestimation of the actual situation. A localized site model again appears to

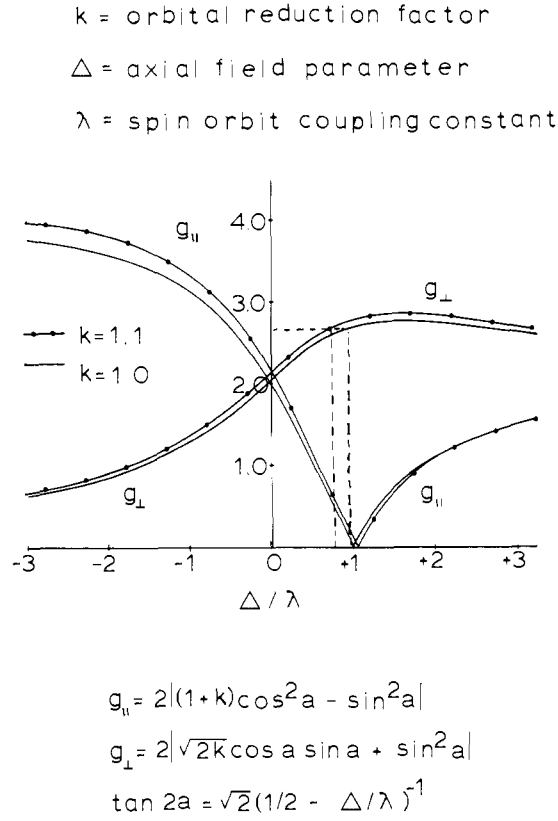


**Figure 6.** Plots of $g_\parallel$ and $g_\perp$ values calculated as a function of the ratio of the tetragonal field parameter Δ and the spin-orbit coupling constant λ for orbital reduction factors, $k$, of 1.0 and 1.1. The dashed lines show that for a $g_\perp$ of 2.68, $g_\parallel$ is expected to be small and $\Delta/\lambda \simeq 1$. The data for $k$ = 1.1 gives the better fit for an isotropic $g$ value of around 2.00, with a $g_\parallel$ = 0.55.

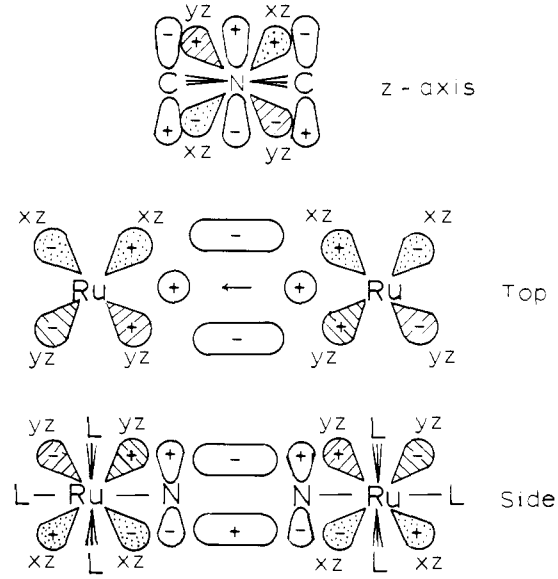


**Figure 7.** Molecular orbitals probably involved in the electron transfer process. Shown here are the $d_{xz}$,$d_{yz}$ orbital manifolds on the two metal centers oriented as indicated by the x-ray crystal structure[8] with respect to the lowest π* orbital of the pyrazine bridge. For clarity, the lobes of the $d_{xz}$ orbitals have been filled in with dots and the lobes of the $d_{yz}$ orbitals have been filled in with lines. Orientations shown are the view looking parallel to the pyrazine ring (labeled side), the view looking down on top of the pyrazine ring (top), and the view along the $z$ axis of the molecule as seen from the interior of the pyrazine ring (as indicated by the arrow in the top view).

be an appropriate model for describing the system. Based on the orbital picture presented above, it is likely that the electron

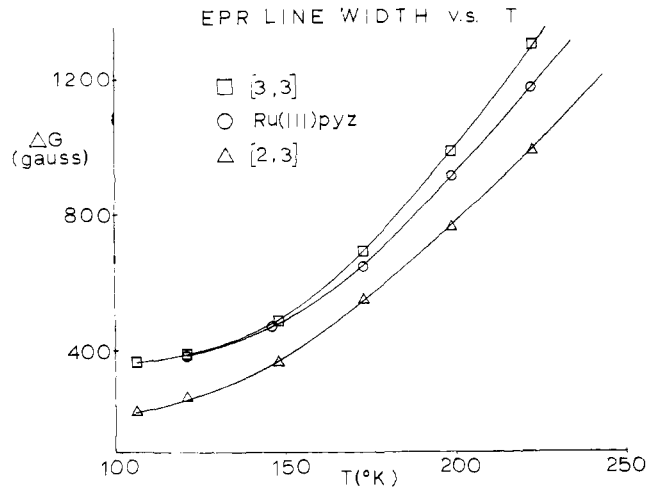


**Figure 8.** EPR line widths of the [2,3]pyr and [3,3]pyr dimers and the $Ru^{III}$pyr monomer as a function of temperature.

transfer process between the localized metal sites involves transfer through the lowest unoccupied molecular orbital of the pyrazine. An electron transfer mechanism involving the pyrazine $\pi^*$ orbitals would have been unlikely if the unpaired electron had been found to be in the $d_{xy}$ orbital instead of $d_{xz}$, $d_{yz}$, since $d_{xy}$ is completely orthogonal to the entire set of orbitals on the pyrazine bridge.

More information concerning the nature of the potential barrier between the metal centers in the [2,3]pyr dimer can be obtained by looking at the charge transfer bands in the electronic spectrum of the complex, since they can be used to gauge the orbital overlap between the Ru(II) center and the bridge. Taube[1] has explained how the shift observed in the most intense charge transfer band in going from the [2,2]pyr dimer to the mixed valence [2,3]pyr dimer is consistent with the localized site model presented above. This shift apparently is a reflection of considerable overlap between the Ru(II) centers and the pyrazine bridge. This orbital interaction is expected to be stronger for Ru(II) than for Ru(III) if the lowest $\pi^*$ orbital on pyrazine is comparable in energy to the d orbital manifold on Ru(II). The d orbitals on Ru(III) are much lower in energy than those on Ru(II) if the coordination spheres about the two metals are the same. The increased overlap in the [2,2] dimer drives the energy of the lowest pyrazine based $\pi^*$ orbital above the level found for the [2,3] dimer, and drives the Ru(II) d orbitals to lower energies. This shifts the metal → ligand charge transfer band to higher energies in going from [2,3] to [2,2]. This effect is not observed in the analogous 4,4′-bipyridyl bridged dimer[15] because the lowest $\pi^*$ orbital for this bridge is considerably higher in energy than that of the pyrazine bridge and would not be expected to interact significantly with either the Ru(II) or Ru(III) d orbitals. It is interesting to note that the intervalence transfer band for the 4,4′ bridged system appears around 1000 nm,[16] indicating that the thermal barrier to electron transfer is much higher for this system than for the pyrazine bridged case. This may be due in part to the reduction in overlap observed between the Ru(II) center and the bridge. Electronic factors may be assisting in the electron transfer from the Ru(II) center to the bridge even though they are of little consequence in assisting in the transfer from the bridge to the Ru(III) center. In terms of these electronic effects, we agree with the conclusions of Ratner, who points out that for these particular ruthenium dimers, the most important component of the effective bonding overlap integral (see previous discussion) is the energy difference between the metal-based and bridge-based orbitals rather than the spatial overlap between the orbital sets as reflected in the tunneling integrals $H^1_{BL_1}$ and $H^1_{BL_2}$.

**Variable Temperature EPR and NMR Studies.** It has now been established that there is a finite barrier to thermal electron transfer in the [2,3]pyr dimer. We have a fairly good idea of what the ground-state molecular orbital of the complex is like. However, no clear picture has yet emerged as to the nature and magnitude of the potential barrier. The rate of electron transfer between the metal centers has yet to be determined. In an attempt to determine the rate of electron transfer as a function of temperature and learn more about this barrier, we looked at the EPR and NMR spectra of these ruthenium compounds as a function of temperature. The major experimental parameter of interest in both of these experiments is the line width of the observed resonance as a function of temperature, since changes in the line width can be indicative of the exchange broadening or exchange narrowing associated with a dynamic rate process.

The results of the variable temperature EPR experiments are shown in Figure 8. The species studied as a function of temperature were pure powders of the [2,3] and [3,3] dimers and the $Ru^{III}$pyr monomer. None of the resonances for these species show appreciable line broadening from 8 K up to 50 K. At liquid nitrogen temperatures, all three resonances are broader. The $g_x$ and $g_y$ components of the $g_\perp$ feature for the [2,3] complex coalesce into a single peak due to this broadening. From liquid nitrogen up to 223 K all three resonances show extreme line broadening as the temperature is raised, and eventually broaden into the baseline. At all temperatures at which line widths were measured, the [2,3] resonance is sharper than the other two by roughly 200 G.

Clearly, the line shapes observed here cannot be explained on the basis of a simple exchange process. The dramatic broadening with temperature seen for all three species is dominated by the effects of the large spin-orbit coupling constant found for Ru(III). As the temperature is raised, lattice vibrations, or phonons, are able to couple the orbital angular momentum on the metal with the electron spin, dramatically increasing the relaxation efficiency for metals having a large spin-orbit coupling constant. The result of this coupling is increasingly shorter spin relaxation times and substantially broader EPR lines. The large spin-orbit coupling constant for Ru(III) makes it difficult to study any ruthenium-containing compounds via EPR techniques at temperatures above liquid nitrogen. The difference in line widths between the [2,3] species and the other two compounds can be attributed to dipolar broadening effects. The concentration of paramagnetic centers in the lattice gives rise to this broadening effect, and is expected to be less for [2,3]pyr dimer than for either of the other two compounds.

It would appear from the results discussed above that the electron transfer process is not a dynamic process on the EPR time scale. To determine whether the rate is fast or slow on the EPR time scale, we need to compare our results to those reported in the literature for mixed valence compounds which are known to have rates of electron transfer which are both fast and slow on the EPR time scale. The mixed valence biferrocenes[22-24] include compounds which meet this criterion. The biferrocenes of interest are those for which both EPR and Mossbauer data are available. For these compounds, the Mossbauer data are fairly definitive in distinguishing whether or not the unpaired electron is moving between the metal centers at a rate which is fast or slow on the Mossbauer time scale of ca. $10^7$ $s^{-1}$. The EPR spectra of the biferrocenes which are demonstrated to be delocalized on the Mossbauer time scale show two major changes when compared to localized biferrocenes: (1) there is a collapse in the $g$ value anisotropy, and (2) there is a dramatic narrowing of the EPR line width. For example, the rate of electron transfer in biferricenium$^+I_3^-$ is slow on the Mossbauer time scale. It shows an EPR signal with a $g_\parallel = 3.58$ and a $g_\perp = 1.72$. This $g$ value anisotropy is

**Table III.** Room Temperature NMR Spectra for the Pyrazine Protons of All Three Oxidation States of the Pyrazine Bridged Dimer (Solvent 2:1 Methanol-$d_4$-$Me_2SO$)

| Species | Pyrazine NMR[a] $\nu$, ppm | $\Delta\nu$, ppm |
|---|---|---|
| [2,2] | 8.0 | 0.03 |
| [2,3] | 19.2 | 3.8 |
| [3,3] | 32 (2) | >10 |

[a] $T$ = 25 °C.

comparable to that found for the monomeric ferricenium$^+I_3^-$ ($g_\parallel$ = 4.35, $g_\perp$ = 1.26). The line width of the $g_\parallel$ component is around 200 G at 12 K. In marked contrast, the EPR spectrum obtained for the compound 1′,6′-diiodoferricenium$^+I_3^-$, which has an electron transfer rate which is fast on the Mossbauer time scale, shows a signal at $g_\parallel$ = 2.75 and a split $g_\perp$ signal centered at $g$ = 1.99, where the line width of the $g_\parallel$ signal is ca. 20 G. Both the collapse of the $g$ value anisotropy and the sharpening of the EPR signal can be rationalized as being due to the unpaired electron spending less time in the vicinity of a given metal center and behaving more like an electron in a free-radical environment. The single unpaired electron in this mixed-valence biferrocene is delocalized on the EPR time scale. The increased thermal electron transfer rate quenches the orbital angular momentum of the unpaired electron and this reduces the $g$-tensor anisotropy and the line width of the EPR signal. The EPR spectra for these EPR-delocalized mixed-valence biferrocenes are readily observed at room temperatures, whereas the EPR spectra for localized species require low temperatures to be detectable.

It has already been shown that for the [2,3]pyr dimer, the collapse in the $g$ value anisotropy is negligible when compared to the [3,3] dimer. The efficiency of line broadening induced by spin-orbit coupling effects has been shown to be comparable for the two systems. Certainly, no changes are observed here which are at all comparable to the changes seen for the biferrocenes. We conclude from this comparison that the rate of intramolecular thermal electron transfer in the [2,3]pyr dimer is slow on the EPR time scale in the temperature range studied. This means that at least in the solid state, the rate of electron transfer is slower than $10^9$ $s^{-1}$ at temperatures below −50 °C. This is consistent with a class II designation for the complex in which there is a finite barrier to thermal electron transfer and localized metal sites.

The EPR results indicate that physical methods used to study the thermal electron transfer process probably need to operate on a time scale which is slower than the EPR time scale of $10^9$ $s^{-1}$ if the transfer is to be observed as a dynamic process. This observation prompted us to study the variable temperature NMR spectra for the [2,3]pyr dimer. A previous NMR study on the dimer done in $Me_2SO$ solutions at room temperature[2] indicates that the electron transfer process is rapid on the NMR time scale of $10^5$ $s^{-1}$. This result was verified by our work at room temperature, which is summarized in Table III. Solutions of all three oxidation states of the dimer were prepared in 2:1 methanol-$Me_2SO$ to enable us to study the NMR resonances at temperatures down to −80 °C. The pyrazine protons of the [2,3] dimer give rise to a single broad resonance which is intermediate in chemical shift and line width to the pyrazine resonances observed for the [2,2] and [3,3] oxidation states. The extreme line width of 3.5 ppm observed for the [2,3] pyrazine resonance is due to the presence of the unpaired electron on the paramagnetic Ru(III) center. This electron is efficient at relaxing the pyrazine protons, giving rise to the broad line shape observed. This electron relaxation process is anticipated to increase in efficiency as the temperature of the system is lowered, since the electron spin is relaxed less efficiently by the orbital angular momentum on the ruthenium center at lower temperatures. This electron spin relaxation has already been demonstrated to change significantly with temperature as reflected in the variable temperature EPR line widths discussed earlier. Unfortunately, the electron spin relaxation effect is expected to dominate line broadening, masking any changes in the line width due to exchange broadening induced by a dynamic electron transfer process. This expectation is realized in the variable temperature line width studies done on the [2,3]pyrazine resonance, which are shown in Figure 9. The line broadening effect observed as the temperature of the system is lowered is much larger than the effect expected on the basis of simple exchange broadening.

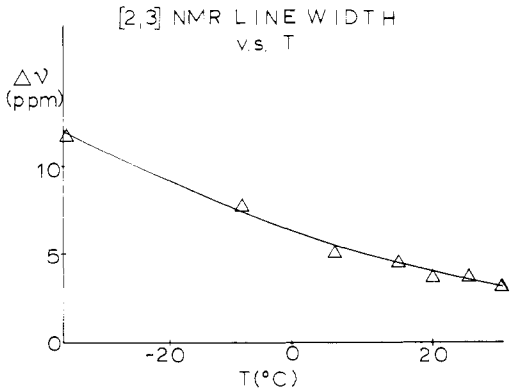


**Figure 9.** NMR line width for the single pyrazine resonances of [2,3]pyr as a function of temperature. The sample was studied in a solution of 2:1 methanol-$d_4$-$Me_2SO$-$d_6$.

However, it is still possible to determine whether the rate of electron transfer is slow or fast on the NMR time scale. If the rate is slow on the NMR time scale, two resonances should be observed for the pyrazine protons. The protons adjacent to the paramagnetic Ru(III) center should give rise to a broad resonance situated in the vicinity of the resonance observed for the [3,3]pyr dimer at around 30 ppm. Those adjacent to the diamagnetic Ru(II) center should give rise to a much sharper resonance at around the 8-ppm position found for the [2,2]pyr dimer. For the actual dimer, a single symmetrical resonance is observed at around 19 ppm which broadens into the baseline by −40 °C. Even at −80 °C, no resonances appear in the spectrum of the [2,3] species which can be attributed to the protons adjacent to the Ru(II) center in a localized mixed valence species. (No resonances are expected to be observable for the Ru(III) center protons owing to the extreme line broadening at low temperatures.) Thus, the rate of electron transfer appears to be fast on the NMR time scale at all temperatures studied. In solution, the electron transfer appears to be faster than $10^5$ $s^{-1}$ at temperatures as low as −80 °C.

The conclusions of the rate data obtained in the EPR and NMR variable temperature experiments do not enable us to determine exactly what the rate of thermal electron transfer between the metal centers in the [2,3]pyr dimer is. For solid samples, the rate is slow on the EPR time scale of $10^9$ $s^{-1}$. In solution, the rate is fast on the NMR time scale of $10^5$ $s^{-1}$. On the basis of this study, it is impossible to estimate the contribution that the phase, or outer coordination sphere around the [2,3] cation, makes to the energy barrier which determines the rate of electron transfer. It is possible that the results are dominated by this effect.

Assuming that the phase change has a minor effect on this system (vide infra), we can use the rate data collected in the EPR and NMR experiments to calculate crude limits which bracket the magnitude of the energy barrier by using the Arrhenius equation:

$$3.4 \text{ kcal/mol} < E_{\text{thermal}} < 6.7 \text{ kcal/mol}$$

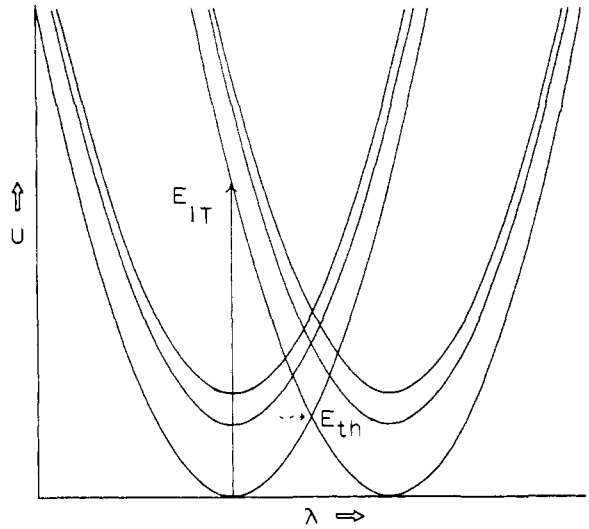


**Figure 10.** Harmonic potential well structure resulting from a consideration of all three Kramer's doublets on the Ru(III) center in the mixed-valence pyrazine bridged dimer. Energy levels shown for the three Kramer's doublets are those calculated on the basis of the $g$ values observed in the EPR spectrum of the complex. $W_0 = 210\ cm^{-1}$, $W_+ = 940\ cm^{-1}$, $W_- = -1150\ cm^{-1}$. The ground-state potential wells correspond to $W_-$. The I.T. band energy of 6369 $cm^{-1}$ is roughly three times the total energy separation of the three Kramer's doublets, which is 2090 $cm^{-1}$.

These limiting values for the magnitude of the energy barrier are consistent with all of the previous experimental conclusions reported in Table I except for the IR results. There are several bands in the IR spectrum of the 5+ species which are intermediate in position between similar bands in the 4+ and 6+ species.[1,7] This has been interpreted to mean that the unpaired electron in the system must be delocalized on the IR time scale of $10^{13}\ s^{-1}$. However, other interpretations are possible. For example, a single vibrational mode could be observed if the transitions associated with one metal center are much more intense than those associated with the other metal center, or if the differences in the frequencies for the [2,2] and [3,3] species are dominated by lattice energy effects. IR studies done on several ruthenium-ammine systems indicate that the latter effect might best explain the IR data. The position of $\rho NH_3$ for $[((NH_3)_5Ru)_2N_2]^{4+}$ ranges from 768 to 798 $cm^{-1}$ depending on the counterion used.[25] IR data reported by Taube[1] indicate that for a series of complexes $[(NH_3)_5RuL]^{2+,3+}$, $\rho NH_3$ can range from 750 to 800 $cm^{-1}$ for Ru(II) centers and from 780 to 820 $cm^{-1}$ for Ru(III) centers. Note that the ranges overlap. If both the Ru(II) and Ru(III) centers find themselves in similar lattice environments, perhaps the separation in their IR frequencies can become so small that bands for each metal center would not be distinguishable. This might be a problem, especially if the bands arising from the Ru(II) and Ru(III) centers are of dissimilar intensities.

The Hush theory prediction for the magnitude of the energy barrier also falls within our experimentally determined limits. However it is important to note at this stage that the Hush theory, although useful from a pedagogical standpoint, oversimplifies the complexities of the electron transfer process in mixed valence compounds. These complexities are reflected in the inadequate agreement between theory and experiment in describing the behavior and appearance of the intervalence transfer band in the [2,3]pyr dimer and other mixed valence compounds.

One oversimplification involves the use of a simple dielectric continuum model for describing the contribution to the vibronic barrier due to the outer coordination sphere around the mixed valence cation. According to this model, the effect of the solvent on the energy of the intervalence transfer transition is given by the equation

$$E_{outer} = \left(\frac{1}{a_{III}} + \frac{1}{a_{II}} - \frac{1}{d}\right) e^2 \left(\frac{1}{n^2} - \frac{1}{D}\right) \qquad (7)$$

where $E_{outer}$ is the outer-sphere Franck-Condon activation energy, $a_{III}$ and $a_{II}$ are the diameters of dielectric saturation about the Ru(III) and Ru(II) centers, $d$ is the distance between the metal centers, $e$ is the electronic charge, $n$ is the refractive index, and $D$ is the static dielectric constant. The solvent dependence predicted by this equation can fail under two extreme sets of conditions. It has recently been demonstrated[26] that in certain binuclear mixed-valence copper complexes, solvent coordination to the metal centers determines the rate of thermal electron transfer between the metal sites. For these systems, the solvent actually has access to the inner coordination sphere of the metal and can play a dominant rather than a secondary role in determining the magnitude of the net energy barrier. The other extreme case is perhaps best illustrated by the [2,3]pyr dimer itself. Here, the model can break down if the magnitude of the energy barrier is near the lower limit of 3.4 kcal/mol indicated by our experiment on the [2,3] system. If the barrier is low enough, the rate of electron transfer could exceed $10^{10}\ s^{-1}$ at room temperature (even though it appears to be slower than $10^9\ s^{-1}$ at −50 °C). Dielectric relaxation studies which have been carried out on a number of the solvents used to determine the solvent dependence of the I.T. band indicate that the relaxation times associated with molecular tumbling in these polar solvents is on the same order of magnitude as or slower than this rate. In other words, the rate of the electron transfer process could be faster than the response time required for reorganization of the solvent molecules. As far as the solvent is concerned, the electron appears to be completely delocalized, causing the solvent molecules to orient themselves in a symmetrical fashion around the entire cation rather than taking different orientations around the Ru(II) and Ru(III) sites.[27] Under these conditions, the solvent would be expected to make a minimal contribution to the energy barrier to electron transfer. This barrier would be essentially the same as the barrier found in the solid state if the anions in the lattice are arranged symmetrically about the entire cation rather than being concentrated about the Ru(III) center. The crystal structure reported byBeattie[8]et al. indicates disordered anions and thus is inconclusive regarding the symmetry, at least when the counterions are halides. Minimal solvent effects may be indicative of electron transfer processes which are faster than around $10^{10}\ s^{-1}$ and may be used to help establish the rate of thermal electron transfer. Systems such as the 4,4′-bipyridyl bridged system which show the predicted solvent dependence probably have electron transfer rates which are slow with respect to solvent reorganizational times.

Another, and a more serious, oversimplification inherent in the Hush theory involves the use of completely harmonic potential wells to describe the vibronic potential energy curves centered on the two metals of the mixed-valence dimer. Anharmonicities in the wells need to be considered. These can arise for a variety of reasons. The vibronic potential is more complex than presented in the Hush theory, being produced by a linear combination of all of the vibrational modes of the molecule rather than a single idealized vibration. The potential well formed by this combination of vibrations could be considered as the linear combination of the harmonic potentials associated with each vibration, but this linear combination need not be harmonic. Another problem associated with using a harmonic potential is that such a potential is really only a good approximation to a vibrational potential well for states lying in the bottom of the well. For excited vibrational states such as those involved in the intervalence transfer transition, this potential is probably better described using a potential function such as the Lennard-Jones potential. Finally, the presence of

metal-metal interactions and other electronic effects can lead to distortions in a purely vibronic potential as discussed in the introduction (see Figure 1). In addition to worrying about the shapes of the potential wells, one should also consider the number of potential wells which can have a bearing on the thermal electron transfer process. In particular, it is unclear what the effect of having several electronic states between the ground state and the excited states involved in the intervalence transition is. For the [2,3]pyr dimer, we have already seen that there are three Kramer's doublets associated with the Ru(III) center. Each of these doublets has a vibronic potential well associated with it. Calculations based on the EPR results presented earlier show that the first excited doublet occurs at an energy which is around one-quarter of the energy of the intervalence transfer transition, and that the highest excited doublet is at a level above the ground state by around one-third the energy of the intervalence transfer transition. If all of these potential wells are considered to be harmonic, a complex potential well structure is the result, as illustrated in Figure 10. Add to this complexity the possibility of anharmonicity as discussed above, and it is easy to see how a strict Hush theory approach can lead to some erroneous conclusions. It is not really surprising that the bandwidths observed for intervalence transfer transitions often fail to adhere to the Hush theory predictions, or that observed rates for thermal electron transfer have been found to contradict predictions based on the energy of the intervalence transfer band.

The final problem anticipated with the Hush theory is in its application over a wide range of temperatures. The Hush model is derived for the high-temperature limit where $2RT > h\nu$, where $h\nu$ is the energy associated with the metal-ligand vibrational transitions in the mixed-valence complex. As Taube[1] points out, $h\nu \simeq 2RT$ at room temperature for [2,3]pyr dimer, as well as for other mixed-valence compounds containing heavy transition metals.

Also, the Arrhenius equation used in this and other papers to relate the rate of the electron transfer to the magnitude of the potential energy barrier should technically only be applied in the limit of high temperatures where Boltzmann statistics are valid. Quantum statistical models will have to be developed to describe the behavior of the system at low temperatures. Quantum mechanical tunneling through the barrier also needs to be considered, especially in the limit of low temperatures.

It is obvious that many questions remain to be answered concerning the rate, the mechanism, and the nature of the energy barrier to electron transfer in the [2,3]pyr dimer. The unusual electrochemical stability of the [2,3] species is also poorly understood at this time.[1] It is hoped that further research on this and other mixed valence species will eventually lead to a fuller understanding of these phenomena.

## Experimental Section

**Compound Preparation.** Synthesis of μ-pyrazine-decaamminediruthenium(II) *p*-toluenesulfonate (or [2,2]pyr) was carried out using standard literature methods[1,15] involving reduction of chloropentaammineruthenium(III) chloride with amalgamated zinc in the presence of a stoichiometric amount of pyrazine, followed by addition of a concentrated solution of sodium tosylate. All operations were carried out under argon in deoxygenated water. The $PF_6$ salt was obtained in a similar fashion using concentrated aqueous solutions of ammonium hexafluorophosphate to precipitate out the cation instead of aqueous sodium tosylate.

μ-Pyrazine-decaammineditruthenium(III) *p*-toluenesulfonate ([3,3]pyr) was synthesized in a similar fashion, except that the solution was treated with an excess of bromine water to oxidize the ruthenium centers before addition of the solution containing the tosylate counterion.

Pyrazinepentaammineruthenium(III) *p*-toluenesulfonate ((Ru(III)pyr) was prepared in an identical fashion with [3,3]pyr except that a tenfold excess of pyrazine was used instead of a stoichiometric amount.

μ-Pyrazine-decaammineditruthenium(5+) was synthesized according to the literature method[1] and by taking a stoichiometric mixture of [2,2]pyr and [3,3]pyr and recrystallizing the mixture in deoxygenated water, taking advantage of the large conproportionation constant of $10^6$ found for the equilibrium [2,2]pyr + [3,3]pyr ⇄ [2,3]pyr. Doped powders of [2,3]pyr in diamagnetic [2,2]pyr used in the ESR experiments were made by adding less than a stoichiometric amount of bromine, silver tosylate, or [3,3]pyr to aqueous solutions containing the [2,2]pyr cation.

UV-visible spectra of all compounds were run on a Cary 14 spectrometer and were found to agree with results reported in the literature. Doping levels in the doped powders used in the EPR experiments were estimated by looking at the relative intensities of the major charge transfer band at around 550 nm and the intervalence transfer band at 1570 nm. Doping levels of 10–20% gave optimal ESR results.

**Physical Methods.** Variable temperature (4.2–290 K) magnetic susceptibility measurements were carried out on a Princeton Applied Research Model 150A vibrating-sample magnetometer as reported previously.[23]

Variable temperature EPR experiments were run on a Varian E-9 spectrometer equipped with an Air Products Heli-tran cryogenic system for measurements at temperatures between 6 and 50 K. Temperature control in the temperature range between liquid nitrogen temperature and room temperature was achieved using a Varian temperature controller. Samples were run as pure powders and doped powders prepared as mentioned above and as $10^{-2}$ M frozen solutions in 1:1 $Me_2SO$-glycerol.

Variable temperature NMR results were obtained on a Jeolco Fx-60 Fourier transform spectrometer equipped with a Jeolco temperature controller. Samples were run as $2 \times 10^{-2}$ M solutions in 2:1 methanol-$d_4$-$Me_2SO$-$d_6$ (99.5 atom % D, Merck Sharp and Dohme).

**Acknowledgment.** The authors wish to acknowledge support of this research by the donors of the Petroleum Research Fund, administered by the American Chemical Society, and the National Institutes of Health Grant HL13652. D. N. Hendrickson also gratefully acknowledges the support provided by the A. P. Sloan Foundation Fellowship and the Camille and Henry Dreyfus Teacher-Scholar Award.

## References and Notes

(1) C. Creutz and H. Taube, *J. Am. Chem. Soc.*, **91**, 3988 (1969); **95**, 1086 (1973).
(2) J. Elias and R. S. Drago, *Inorg. Chem.*, **11**, 415 (1972).
(3) C. Creutz, M. L. Good, and S. Chandra, *Inorg. Nucl. Chem. Lett.*, **9**, 171 (1973).
(4) P. Citrin, *J. Am. Chem. Soc.*, **95**, 6472 (1973).
(5) I. Treitel, "Electronic Structures of Ligand Bridged Ruthenium and Cobalt Binuclear Complexes", Ph.D. Thesis, California Institute of Technology, 1971.
(6) T. Strekas and T. Spiro, *Inorg. Chem.*, **15**, 974 (1976).
(7) J. Beattie, N. Hush, and P. Taylor, *Inorg. Chem.*, **15**, 992 (1976).
(8) J. Beattie, C. Raston, and A. White, *J. Chem. Soc., Dalton Trans.*, 1121 (1977).
(9) B. Mayoh and P. Day, *J. Am. Chem. Soc.*, **94**, 2885 (1972).
(10) B. Mayoh and P. Day, *Inorg. Chem.*, **13**, 2273 (1974).
(11) N. Hush, *Prog. Inorg. Chem.*, **8**, 391 (1967).
(12) M. Robin and P. Day, *Adv. Inorg. Chem. Radiochem.*, **10**, 248 (1967).
(13) M. Ratner and M. J. Ondrechen, *Mol. Phys.*, **32**, 1233 (1976).
(14) J. Stanko, H. Peresie, R. Bernheim, and P. Wang, *Inorg. Chem.*, **12**, 634 (1973).
(15) D. K/ Lavellee and E. B. Fleischer, *J. Am. Chem. Soc.*, **94**, 2583, 2599 (1972).
(16) G. M. Tom, C. Creutz, and H. Taube, *J. Am. Chem. Soc.*, **96**, 7827 (1974).
(17) K. Stevens, *Proc. R. Soc. London, Ser. A*, **219**, 542 (1953).
(18) H. Kamimura, *J. Phys. Soc. Jpn.*, **11**, 1171 (1956).
(19) B. Bleaney and M. O'Brien, *Proc. Phys. Soc. London, Sect. B*, **69**, 1215 (1956).
(20) R. DeSimone and R. S. Drago, *J. Am. Chem. Soc.*, **92**, 2343 (1970).
(21) R. DeSimone, "Magnetic Studies of Low Spin $d^5$ Transition Metal Complexes", Ph.D. Thesis, University of Illinois, 1970.
(22) D. O. Cowan, G. A. Candela, and F. Kaufman, *J. Am. Chem. Soc.*, **93**, 3889 (1971).
(23) W. Morrison and D. Hendrickson, *Inorg. Chem.*, **14**, 2331 (1975).
(24) W. Morrison, S. Krogsrud, and D. Hendrickson, *Inorg. Chem.*, **12**, 1998 (1973).

(25) A. D. Allen, F. Bottomley, R. A. Harris, V. P. Reinsalu, and C. V. Senoff, *J. Am. Chem. Soc.*, **89**, 5595 (1967).
(26) R. Gagne, C. Koval, and T. Smith, Abstracts, 174th National Meeting of the American Chemical Society, Chicago, Ill., Aug 1977, No. INOR-85.
(27) In terms of eq 7, this is the same as saying that the effective dielectric constant of the solvent, $D_{eff}$, is better approximated by the infinite frequency dielectric constant, $D_\infty$, which measures the polarizability of the solvent, than by the static dielectric constant $D$, which also includes effects caused by the motion of solvent dipoles due to molecular tumbling. Note that $D_\infty \simeq n^2$.

# The Molybdenum Site of Nitrogenase. 2. A Comparative Study of Mo–Fe Proteins and the Iron–Molybdenum Cofactor by X-Ray Absorption Spectroscopy

**Stephen P. Cramer,[1a] William O. Gillum,[1a] Keith O. Hodgson,*[1a] Leonard E. Mortenson,[1b] Edward I. Stiefel,[1c] John R. Chisnell,[1d] Winston J. Brill,[1d] and Vinod K. Shah[1d]**

*Contribution from the Department of Chemistry, Stanford University, Stanford, California 94305, Department of Biological Sciences, Purdue University, West Lafayette, Indiana 47907, Charles F. Kettering Research Laboratory, Yellow Springs, Ohio 45387, and Department of Bacteriology and Center for Studies of Nitrogen Fixation, University of Wisconsin, Madison, Wisconsin 53706.*
*Received December 1, 1977*

**Abstract:** Recently, the Mo environment in lyophilized MoFe protein from *Clostridium pasteurianum* has been structurally characterized by x-ray absorption spectroscopy measurements. As a further step in elucidating the structure and relationship of the Mo environment in other species, the MoFe component from *Azotobacter vinelandii* has been studied. The K-edge Mo x-ray absorption spectra for the intact crystalline MoFe component and for the cofactor (FeMo-co) derived from this component have been recorded. There exists a striking similarity in both the edge and EXAFS regions of the spectra between the *Clostridium* and *Azotobacter* data. Detailed analysis leads to the conclusion that the Mo environment is not significantly perturbed by the lyophilization process and that the Mo environment in the protein from *Azotobacter* has the same environment at the Mo site—an as yet chemically unknown Mo–Fe–S cluster. Finally, the studies show that the basic features of the Mo environment in the cofactor are preserved during the extraction process and that the intact protein and the cofactor share quite similar Mo sites. These data lend quantitative support to the idea of a common Mo site in the nitrogenase MoFe proteins.

## Introduction

Because of its spectroscopic obscurity, virtually nothing has been known until recently about the molybdenum site in the nitrogenase Mo–Fe protein (also known as component I).[2a] As a first step in the application of x-ray absorption spectroscopy[2b] to the study of molybdenum in nitrogenase, the x-ray absorption spectrum of lyophilized, semireduced *Clostridium pasteurianum* Mo–Fe protein (Cpl) was recorded and analyzed.[3] Furthermore, the absorption edge region spectra for this protein in the fully reduced, semireduced, dye-oxidized, and air-oxidized states were obtained and compared with edges of known Mo structures.[3] The combined edge and EXAFS data were interpreted as evidence for a primarily sulfur, non-Mo=O nitrogenase Mo environment, and the EXAFS itself was best explained by postulating a Mo, Fe, S cluster.[3]

Considering the novelty of the spectroscopic techniques involved, the air sensitivity of the nitrogenase enzyme, and the importance of the structural conclusions, it appeared important to reproduce the results of the Cpl investigation on another bacterial nitrogenase. Accordingly, x-ray absorption spectra have been obtained for the *Azotobacter vinelandii* nitrogenase Mo–Fe protein (Avl) and for the iron–molybdenum cofactor (FeMo-co) isolated from Avl.[4] The Avl and FeMo-co spectra are quite similar to those previously obtained on Cpl, indicating similar molybdenum environments in all three samples. These results therefore reinforce the previous Mo, Fe, S cluster hypothesis initially proposed on the basis of the Cpl data.[3] The Avl spectra demonstrate that useful EXAFS data can be obtained on the Mo–Fe protein under aqueous conditions, thereby making possible a variety of interesting experiments. Furthermore, although the current FeMo-co spectra are of lower quality than the intact protein spectra, it has been verified that the cofactor preserves the essential features of the nitrogenase Mo site. Further study of this material at higher concentrations should yield a wealth of detailed structural information about the metal sites of nitrogenase.

## Experimental Section

**Avl Preparation and Handling.** The Avl protein was prepared at the Charles F. Kettering Research Laboratory (CFKRL) by modifications of procedures due to Bulen and LeComte[5a] and Shah and Brill.[6] In this procedure the final step involves crystallization in 0.046 M NaCl in Tris buffer (pH 7.4) at 38 °C. The precipitated crystals were washed with 0.046 M NaCl in 0.025 M Tris buffer (pH 7.4) containing 1 mg/mL $Na_2S_2O_4$ and centrifuged anaerobically at 12 000 *g* for 10 min to yield a soft pellet. The sealed centrifuge tube was taken into an argon-filled Vacuum Atmospheres box where a gas-tight syringe was used with a 16-gauge cannula to transfer the paste from the centrifuge tube to the Lucite sample cell. The sealed cell was frozen in dry ice and kept at dry ice temperatures throughout shipment and data collection until returned to CFKRL for analysis. The cell was opened in the argon-filled box and the protein dissolved in 0.25 M NaCl in 0.025 M Tris buffer (pH 7.4). It was then analyzed in parallel with a small amount of sample from the same preparation which had been stored in liquid $N_2$.

The unirradiated protein had a specific activity of 1300 nmol $C_2H_4$ $min^{-1}$ $mg^{-1}$ of protein while that which had been subject to x-ray spectroscopy had an activity of 1100 nmol $C_2H_4$ $min^{-1}$ $mg^{-1}$ protein. Polyacrylamide gel electrophoreses, loaded with 90 $\mu g$ of protein on 5-mm diameter cylindrical gels, were identical for the two samples, showing a single large band when stained with Coomassie brilliant blue and a very faint trailing bond which is not visible in photographs of the gels. The EXAFS sample contained 6.2 nmol of Mo and 102

0002-7863/78/1500-3814$01.00/0 